Monthly Notices of the ROYAL ASTRONOMICAL SOCIETY
MNRAS **494,** 3937–3949 (2020) doi:10.1093/mnras/staa927

A new spectroscopic analysis of the massive O + O type binary HD 54662 AB

R. H. Barbá [1★] C. Sabín-Sanjulián,[1] J. I. Arias [1★] R. C. Gamen [2,3] N. I. Morrell [4] G. Ferrero,[2,3] J. Maíz Apellániz [5] C. Putkuri,[2,3] S. Simón Díaz [6,7] T. S. Boyajian [8] A. W. Fullerton[9] and M. V. McSwain[10]

[1]*Departamento de Astronomía, Universidad de La Serena, Av. Juan Cisternas 1200 Norte, La Serena, Chile*
[2]*Instituto de Astrofísica La Plata, CONICET-UNLP, Paseo del Bosque s/n, 1900 La Plata, Argentina*
[3]*Facultad de Ciencias Astronómicas y Geofísicas, UNLP, Paseo del Bosque s/n, 1900 La Plata, Argentina*
[4]*Las Campanas Observatory, Carnegie Observatories, Casilla 601, La Serena, Chile*
[5]*Centro de Astrobiología (CSIC-INTA), Campus ESAC, Camino Bajo del Castillo s/n, E-28692 Villanueva de la Cañada, Madrid, Spain*
[6]*Departamento de Astrofísica, Universidad de La Laguna , E-38205 La Laguna, Tenerife, Spain*
[7]*Instituto de Astrofísica de Canarias, E-38200 La Laguna, Tenerife, Spain*
[8]*Department of Physics and Astronomy, Louisiana State University, Baton Rouge, LA 70803, USA*
[9]*Space Telescope Science Institute, 3700 San Martin Drive, Baltimore, MD 21218, USA*
[10]*Department of Physics, Lehigh University, 16 Memorial Drive East, Bethlehem, PA 18015, USA*

Accepted 2020 March 13. Received 2020 March 13; in original form 2019 July 9

ABSTRACT

HD 54662 AB is one of the three O + OB binaries known so far with orbital period longer than 1000 d, offering the opportunity to test scenarios of massive star formation and models of single stellar evolution. Here, we present a detailed study of this system based on new high-resolution spectra and data. A disentangling method is used to recover the individual spectra of the primary and secondary components, which are classified as O6.5 V(n)z and O7.5 Vz, respectively. Combining radial velocity measurements and astrometric data, a new absolute orbit with a period of 2113 ± 9 d and an eccentricity of 0.062 ± 0.008 is determined, confirming previous findings. However, absolute masses of 23.8 ± 1.1 $M_\odot$ for the primary and 20.3 ± 1.1 $M_\odot$ for the secondary are obtained, differing from previous determinations but in reasonable agreement with the spectral types of the stars. Primary and secondary components show remarkably different projected rotational velocities (160 and $\lesssim$40 km s^{-1} , respectively), which is probably related to the formation process of the binary. Contrary to previously interpretations, the star with broader spectral features is the most massive object in the system. Stellar and wind parameters of both stars are derived through quantitative spectroscopic analysis of the disentangled spectra using FASTWIND models, and they are consistent with the current calibrations for O-type stars. Evolutionary masses and ages are also computed with the BONNSAI tool. Ages below 2.5 Ma are obtained, in agreement with the youth expected from their Vz nature.

Key words: stars: atmospheres – binaries: spectroscopic – stars: early-type – stars: fundamental parameters – stars: individual: HD 54662 AB.

1 INTRODUCTION

Multiplicity is a key factor to consider in the evolution of massive stars, as more than a half of these objects are born in binary or multiple systems (Sana et al. 2012; Barbá et al. 2017). For close binary systems, besides the complications inherent to the massive stellar evolution (e.g. rotation and metallicity dependence), one must take into account processes like mass transfer and mergers, which aggregate additional difficulties to the modelling. However, for long-period binary systems the latter processes are not necessarily relevant, since the large separation between components strongly constrains possible binary interactions (Sana et al. 2012). Thus, long-period binaries appear as ideal laboratories to test single-star evolutionary models.

The O-type star HD 54662 AB (HR 2694, $\alpha_{2000} = 07^h09^m20\overset{s}{.}25$, $\delta_{2000} = -10°20'47\overset{''}{.}63$, $V = 6.21$, Ducati et al. 2001; O7 Vz var?, Sota et al. 2014) is the earliest member of the CMa OB1 association in the Seagull Nebula (IC 2177) complex. The radial velocities (RVs) of this star have been studied by many researchers for

★ E-mail: rbarba@userena.cl (RHB); jarias@userena.cl (JIA)

Table 1. Details of the collected spectroscopic data of HD 54662 AB.

Date	Instr. config.	Observat.	R	Range (nm)	n^a
2005 Nov	UVES, 8.2 m	Paranal	41 000	373–500	3
2006 Feb	Echelle, 2.5 m	LCO	40 000	345–985	1
2006 May	REOSC, 2.1 m	CASLEO	15 000	360–610	1
2007 Apr	REOSC, 2.1 m	CASLEO	15 000	360–610	1
2008 Jan	REOSC, 2.1 m	CASLEO	15 000	360–610	1
2008 Feb	REOSC, 2.1 m	CASLEO	15 000	360–610	1
2008 May	FEROS, 2.2 m	La Silla	48 000	357–921	1
2008 Oct	Coude, 0.9 m	KPNO	9000	413–457	1
2008 Nov	Coude, 0.9 m	KPNO	9000	413–457	2
2009 Jan	REOSC, 2.1 m	CASLEO	15 000	360–610	2
2009 May	Echelle, 2.5 m	LCO	40 000	345–985	1
2009 Jun	REOSC, 2.1 m	CASLEO	15 000	360–610	1
2010 May	Echelle, 2.5 m	LCO	40 000	345–985	1
2011 Feb	FEROS, 2.2 m	La Silla	48 000	357–921	1
2011 Apr	Echelle, 2.5 m	LCO	40 000	345–985	1
2011 May	FEROS, 2.2 m	La Silla	48 000	357–921	1
2011 May	Echelle, 2.5 m	LCO	40 000	345–985	1
2011 Aug	UVES, 8.2 m	Paranal	41 000	373–500	1
2011 Oct	Echelle, 2.5 m	LCO	40 000	345–985	2
2011 Dec	Coude, 0.9 m	KPNO	9000	632–702	3
2011 Dec	REOSC, 2.1 m	CASLEO	15 000	360–610	3
2012 Mar	REOSC, 2.1 m	CASLEO	15 000	360–610	1
2012 Mar	UVES, 8.2 m	Paranal	41 000	373–500	1
2012 May	FEROS, 2.2 m	La Silla	48 000	357–921	1
2012 Nov	UVES, 8.2 m	Paranal	41 000	373–500	5
2013 Feb	MIKE, 6.5 m	LCO	33 000	333–940	1
2013 May	Echelle, 2.5 m	LCO	40 000	345–985	1
2015 Feb	REOSC, 2.1 m	CASLEO	15 000	360–610	1
2015 Mar	REOSC, 2.1 m	CASLEO	15 000	360–610	1
2015 May	Echelle, 2.5 m	LCO	40 000	345–985	2

[a]Number of spectra obtained during each specific month.

decades (Plaskett 1924; Conti, Leep & Lorre 1977; Garmany, Conti & Massey 1980; Fullerton 1990). The latter noted that it was actually a double-lined spectroscopic binary, since a broad secondary component was visible in the blue wing of the lines he observed, consistent with a spectral type near O7. The first orbit of HD 54662 AB was determined by Boyajian et al. (2007, hereafter B07). These authors analysed all the RV measurements available at that moment, a total of 67 spanning 85 yr, and obtained an orbital solution for the primary component, characterized by a period $P = 557.8 \pm 0.3$ d and an eccentricity $e = 0.28 \pm 0.04$. The minimum masses derived in that study were $M_1 \sin^3 i = 41.5 \pm 7.6\,M_\odot$ for the primary, unusually high for an O7 star, and $M_2 \sin^3 i = 16.0 \pm 3.4\,M_\odot$ for the secondary. Some years later, Sota et al. (2014) reported that the RV analysis of the high-resolution spectra obtained in the framework of the spectroscopic monitoring of Galactic O and Wolf–Rayet nitrogen stars known as the *OWN Survey* (Barbá et al. 2010, 2017) indicated for this binary system a different, much longer period of 2119 ± 5 d. By the same time, the components of HD 54662 AB were spatially resolved using the VLTI/PIONIER instrument by Sana et al. (2014). An angular separation between components of 2.6 ± 0.24 mas and a brightness difference of 0.23 mag in the H band were determined in this study.

Recently, Le Bouquin et al. (2017, hereafter LB17) combined the capabilities of the VLTI instruments PIONIER, AMBER, and GRAVITY to determine the first apparent orbit of HD 54662 AB. Their orbital solution corresponds to a period of 2103 ± 4.3 d, which confirms the spectroscopic period previously reported by Sota et al. (2014). Surprisingly, the determined eccentricity is rather low ($e = 0.06$) taking into account the very long period of the system. From the apparent orbit and adopting a distance of 1.1 kpc, these authors derived for the system a total mass of $45 \pm 12\,M_\odot$. However, they adopted the B07 RVs to derive absolute masses for the combined spectroscopic and astrometric orbits, and obtained unrealistic masses of $M_A = 316 \pm 168\,M_\odot$ and $M_B = 58 \pm 19\,M_\odot$ for the primary and secondary, respectively, which they attributed to the lack of accurate RV measurements.

The most recent study on HD 54662 AB was done by Mossoux, Mahy & Rauw (2018, MMR18 hereafter), who used a spectral disentangling method to determine a new RV orbital solution. Their orbit is characterized by a period of 2 103 d, consistent with the astrometric period, and an eccentricity of 0.11, i.e. somewhat smaller than the previously derived. Curiously, the solution found by MMR18 yields very low masses for both components (9.7 and $8.2\,M_\odot$ for the primary and secondary, respectively), as well as a large brightness difference between them, contrary to what would be expected for a system composed of, as stated by the authors, two O6.5 V stars.

In this work, we present a new spectroscopic study of HD 54662 AB based on a combination of data from the *OWN Survey*, the literature, and the European Southern Observatory (ESO) Science Archive. Details of the different data sets are given in Section 2. Section 3 describes the disentangling of the composite spectra, the measurement of the RVs, and the new spectral classifications of the components. A new spectroscopic solution as well as a combined visual–spectroscopic orbit is presented in Section 4. The quantitative spectroscopic analysis of the disentangled spectra, yielding stellar and wind parameters for the individual components, is presented in Section 5. Our results are discussed in Section 6 and summarized in Section 7.

2 OBSERVATIONS

This work is mainly based on high-resolution observations obtained within the framework of the *OWN Survey*, complemented by spectra retrieved from the ESO Science Archive and spectra obtained at Kitt Peak National Observatory (KPNO, USA). Details of the observational data sets are presented in Table 1.

The *OWN Survey* data set consists of 28 high-resolution spectra obtained between 2006 and 2015 at three different observatories: the Complejo Astronómico El Leoncito (CASLEO,[1] Argentina), Las Campanas Observatory (LCO, Chile), and ESO/La Silla Observatory (LSO, Chile). At CASLEO, we employed the REOSC SEL[2] Cassegrain spectrograph in cross-dispersion mode. At ESO/LSO, we used the Fiber-fed Extended Range Optical Spectrograph (FEROS; Kaufer et al. 1999) at the ESO/MPI 2.2 m telescope. Two different instrumental configurations were used at LCO: the Échelle spectrograph attached to the 2.5 m du Pont telescope and the Magellan Inamori Kyocera Echelle (MIKE; Bernstein et al. 2003) at the 6.5 m Magellan II Clay Telescope. The KPNO data comprise the series of spectra presented in B07 and a set of additional spectrograms obtained in 2008 and 2011 with the same instrumental configuration described in B07 (see also Table 1). Additionally, the 17 original spectra published by Fullerton (1990) were measured in order to check the consistency of our disentangling procedure. Fullerton's spectra were obtained in 1985 and 1986 at the Coudé

[1]Operated under agreement between CONICET and the Universities of La Plata, Córdoba, and San Juan, Argentina.
[2]Spectrograph Échelle Liège (jointly built by REOSC and Liège Observatory, and on a long-term loan from the latter).

focus of the Canada–France–Hawaii Telescope, in the yellow region of the spectrum, with a resolving power of about 20 000.

The new CASLEO, LCO, and KPNO spectra were processed and calibrated using the standard IRAF[3] routines. The spectra obtained with FEROS were reduced with the standard reduction pipeline, layered in the MIDAS package supported by ESO.

The archival data retrieved from the ESO Archive consist of 10 calibrated spectra obtained with the UVES spectrograph (Dekker et al. 2000) in 2005, 2011, and 2012.[4]

Spectral normalization was performed on each spectrum independently, and they were compared together to check the consistency of the normalization process, which turns out to be satisfactory. As will be seen later, the components of the system have a relatively low amplitude in radial velocity; therefore, the shape of the hydrogen profiles due to the orbital motion of the stars is affected mostly in the core and not in the wings of the lines.

3 DISENTANGLING OF THE COMPOSITE SPECTRUM

3.1 Individual spectra and radial velocities

The line absorption profiles observed in the composite spectrum of HD 54662 AB show one narrow- and one broad-lined stellar component heavily blended. B07 identified the component with sharper absorption lines as the primary star in the system (i.e. the most massive), and the component with broader absorption lines as the secondary. Subsequently, LB17 and MMR18 adopted a similar binary configuration. However, as will be demonstrated forthwith, the hottest and most massive star of the two in the system is the component whose line profiles are broader. Hence, in this work, we refer to the broad-lined component as the primary and designate it with 'A'. Correspondingly, the narrow-lined component is referred to as the secondary and designated with 'B'.

We have applied the method of spectral disentangling developed by González & Levato (2006) to separate the spectra of each stellar component and measure RVs. This algorithm consists of the alternate use of the spectrum of one component to calculate the spectrum of the companion from the composite spectrum. In each step, the spectrum obtained for one star is subtracted from the observed composite spectrum, and then the derived residual spectrum (an approximation to the single-lined spectrum of the companion) is used to measure the RVs of the remaining component and to evaluate its spectrum after combining them properly. These calculations are performed in two steps: the first one evaluates the spectra for each stellar component, and the second one measures the RVs. The calculations in both steps depend on the results of each other, and then they must be run iteratively in order to get the convergence to the representative spectrum for each component. These RVs are measured in each resulting single spectrum by means of a Fourier cross-correlation technique of these spectra and the respective calculated template spectrum, through the IRAF FXCOR task. The resulting RVs are used in a new disentangling iteration, improving the recovering of individual spectra and the corresponding RV determinations.

In the case of HD 54662 AB, we used only the spectrograms obtained with the highest spectral resolution and signal-to-noise ratio, S/N, i.e. those collected at Paranal, La Silla, and Las Campanas observatories, to recover the spectra of the broad-lined primary (A) and the narrow-lined secondary (B) stars. The procedure was applied in the 390–680 nm spectral range, but taken special care in the inspection around the absorption lines used for spectral analysis. We should mention that telluric water lines around He I 5876 Å, and Hα are not an issue because these telluric lines present very narrow profiles which are automatically removed in the combination steps during the spectral disentangling process. In practice, templates for the stars are not needed beforehand to start the disentangling iteration, although the convergence process is greatly improved when appropriate models are provided. We used as initial templates TLUSTY models (Lanz & Hubeny 2003) with solar abundances, $\log g = 4.0$, and $T_{\rm eff}$ ranging from 35 000 to 40 000 K. Initial values for the projected rotational velocities ($v \sin i$) of the stellar components were estimated from the double Gaussian fitting of the He I lines, performed using the IRAF task NGAUSSFIT. The derived values are in the range 30–50 km s^{-1} for star B, and in the range 130–180 km s^{-1} for star A. For each component, we calculated a grid of templates with three different values of $T_{\rm eff}$ and $v \sin i$. Since the observed continuum flux in the composite spectrum is the sum of the contributions of the two stellar components, the spectral features in the individual disentangled spectra appear 'diluted'. The relative brightness of the stars in the H band was determined by Sana et al. (2014), who found $\Delta H = 0.23$ mag, corresponding to a brightness ratio of about 0.82. We assumed that the former brightness ratio is also valid in the optical band. We consider valid for the optical band the luminosity ratio estimated in the NIR because the differential colour $(V - H)$ for stars with spectral types O6.5 V and O7.5 V is 0.0 (see Martins & Plez 2006), which is also consistent for similar $T_{\rm eff}$ obtained for both stars in the quantitative spectral analysis (see Section 5). Because we ignored a priori which of the stellar components was the brightest, we considered two sets of templates: one in which the broad-lined A contributed with the 55 per cent of the total light and the narrow-lined B with the 45 per cent ($L_{\rm B}/L_{\rm A} = 0.45/0.55 = 0.818$), and another in which the light contributions were the opposite ($L_{\rm A}/L_{\rm B} = 0.45/0.55 = 0.818$). The disentangling process converges after 50–100 iterations to similar results for most of the initial templates. The best results were selected by visual inspection of the spectra. We found that the disentangled spectra showing smaller profile distortions are produced from initial models corresponding to a broad-lined A component with higher temperature and brightness contribution.

Fig. 1 shows the individual spectra resulting from the disentangling process. Some distortion of the profiles, especially in the wings of the Balmer lines, can be observed. This type of distortion effects are described by González & Levato (2006) as residuals due to the very low RV amplitude of the binary. Since the determination of the surface gravity is particularly sensitive to the shape of the Balmer wings, this issue must be taken with caution. We will discuss this in Sections 5.2 and 6.2.

As already mentioned, the González & Levato (2006) disentangling method also yields the RVs of both components for each of the used spectra. All the RV measurements and their corresponding errors are listed in Table 2. For the spectra not used to obtain the separated components in the disentangling procedure (i.e. those obtained at CASLEO, KPNO, and CFHT), RVs were determined through the task FXCOR, using the disentangled spectra as templates.

[3] IRAF is distributed by the National Optical Astronomy Observatories, which are operated by the Association of Universities for Research in Astronomy, Inc., under cooperative agreement with the National Science Foundation.

[4] Based on observations made with ESO Telescopes at the La Silla/Paranal Observatory under programmes: 076.A-0860, 087.D-0264, 088.D-0424, and 090.D-0600.

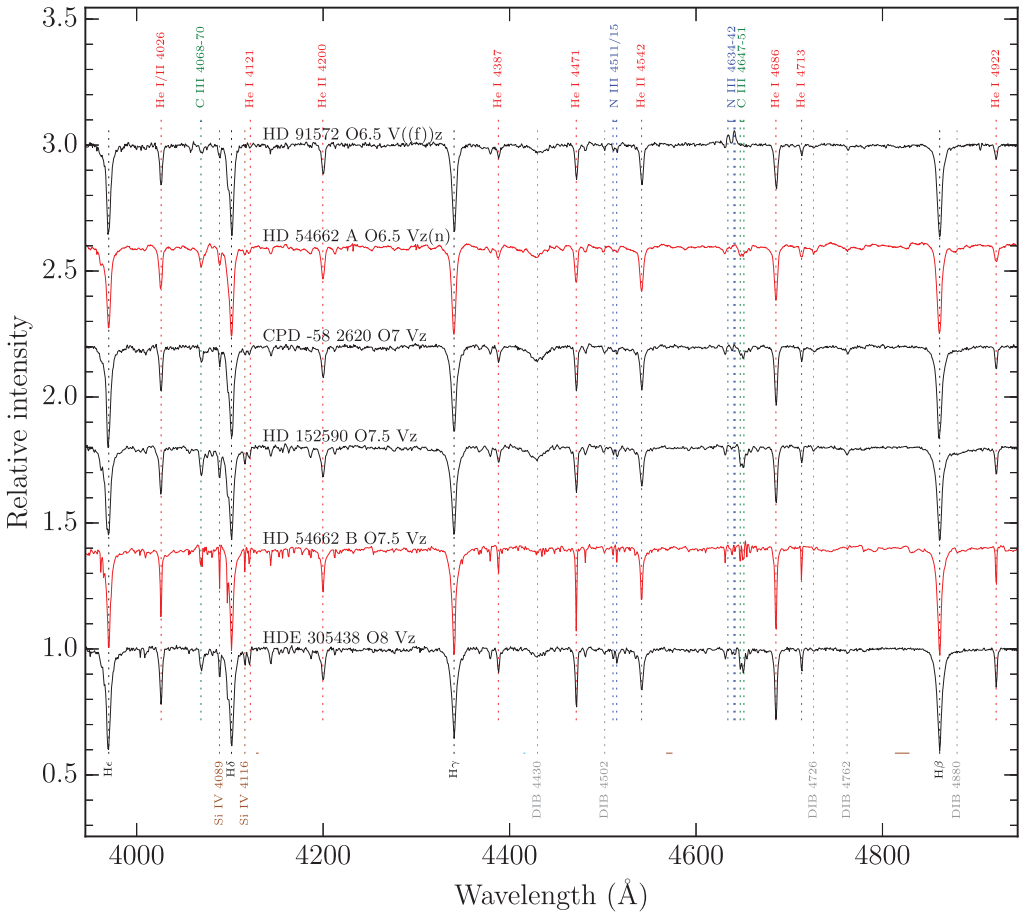

Figure 1. Individual spectra of the components of HD 54662 AB obtained through the disentangling procedure (in red), compared with the GOSSS O-type standards for the corresponding spectral range (in black). Some important stellar spectral features and diffuse interstellar bands (DIBs) are labelled.

Table 2. Radial velocities derived from the disentangling process for both components in HD 54662 AB used in the spectroscopic and 3D orbit.

HJD 2400 000+	RV_A (km s^{-1})	σ_A (km s^{-1})	RV_B (km s^{-1})	σ_B (km s^{-1})
53 701.814	66.6	1.0	12.4	0.5
53 772.543	66.2	1.7	12.3	1.2
54 600.498	13.5	0.5	73.0	0.3
55 337.444	53.0	1.4	30.8	1.0
55 606.537	64.6	0.8	15.4	0.4
55 664.524	65.2	1.0	11.0	0.6
55 671.528	67.2	1.4	12.0	0.8
55 696.468	65.8	0.8	11.9	0.4
55 697.467	66.2	2.1	10.4	1.2
55 796.889	65.8	1.6	9.0	0.9
55 844.890	67.7	1.0	9.0	0.6
55 845.879	67.6	1.1	11.3	0.8
56 008.599	58.3	1.7	19.3	1.2
56 067.464	53.6	0.8	26.1	0.4
56 259.801	38.8	1.3	41.9	0.8
56 324.609	35.2	1.8	50.0	1.0
56 433.457	24.0	1.7	58.1	1.0
57 155.479	29.6	2.1	53.5	1.0
57 157.466	32.6	2.1	51.2	1.0

These RV measurements and errors are shown in Tables A1 and A2 in the appendix. These RVs are used to obtain the period of the system and to confirm the consistency of the orbital solution obtained with RVs derived from the highest resolution spectra.

3.2 Spectral classification

Using the individual spectra resulting from the disentangling process, the MK spectral types of the A and B components were determined. For this purpose we used MGB (*Marxist Ghost Buster*, see Maíz Apellániz et al. 2012), an IDL code that allows the user to compare visually the unknown spectrum with a library of O-type standard stars defined in the framework of the GOSSS project (Maíz Apellániz et al. 2016, and references therein). For visualization purposes, in Fig. 1 we included the spectra of some of the GOSSS standards (in black), along with the spectra of the components A and B (in red).

The features observed in the spectrum of component A are significantly broadened. We assigned to this star the spectral type O6.5 V(n)z, where the qualifier (n) indicates that the lines are rotationally broadened by $v \sin i \sim 200$ km s^{-1} (Sota et al. 2011). On the other hand, the qualifier *z* refers to the unusually strong He II 4686 Å absorption. Using the quantitative criterion by Arias et al. (2016), the *z*-parameter, defined as the ratio between the EW(He II 4686) and the maximum of EW(He II 4542) and EW(He I 4471), is calculated to be 1.10, which means that this star is a marginal O Vz object.

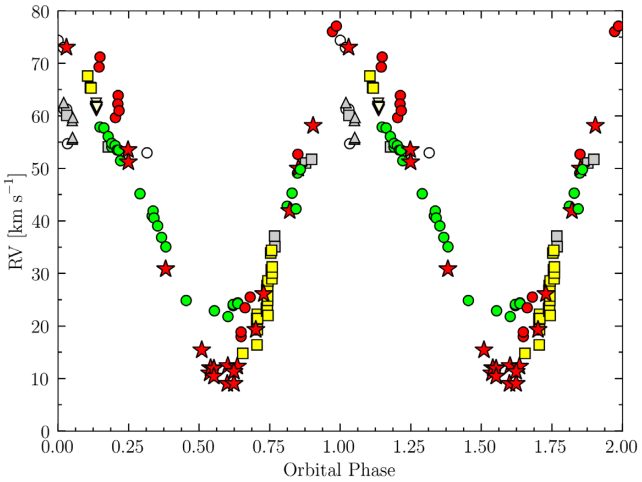

Figure 2. RVs for the narrow-lined component B of HD 54662 AB folded with a period of 2098 d. Different symbols correspond to: (◯) Plaskett (1924); (■, grey) Stickland & Lloyd (2001); (▲) Garmany et al. (1980); (●, green) MMR18. This work: (⋆) LCO, La Silla, Paranal; (●, red) CASLEO; (■, yellow) KPNO; and (▼) CFHT.

The absorption lines observed in the spectrum of the B component are much narrower. We classified this star as O7.5 Vz, with a *z*-parameter of 1.17.

4 ORBITAL SOLUTIONS

4.1 The new spectroscopic orbit

First, we explore the consistency of the period previously found by us and those quoted in the literature. To search for periodicities, we used all the measured RVs (Table 2 and appendix) for the narrow-lined component, and RVs available from the literature (Plaskett 1924; Garmany et al. 1980; Stickland & Lloyd 2001; Mossoux et al. 2018). We have used the MARMUZ code (Marraco & Muzzio 1980) and the Lomb–Scargle method (Scargle 1982), as implemented by NASA Exoplanet Archive Periodogram Service,[5] obtaining most probable values of 2092 and 2098 d, respectively, in very good agreement with previous findings. Fig. 2 shows all the available RVs folded with the period of 2098 d. The difference in RV amplitudes as determined by different data sets is clearly noted. Although the RV determinations spanning about 33 000 d, earlier results obtained from photographic plates are not considered for the final orbital solutions because they are obtained from blended stellar profiles, very different wavelengths (like far-UV), etc.

Adopting $P = 2098$ d as the initial value for the period, we used the GBART[6] code to derive a new spectroscopic orbital solution. To begin, we used all the RV determinations for both components, weighting them according to the resolving power of the spectrum. Specifically, we assigned a weight of 1.0 to LCO, La Silla, and Paranal data, 0.5 to CASLEO observations, and 0.3 to KPNO and CFHT observations. However, the initial trial for the orbital calculation showed that the residuals corresponding to the RVs from CASLEO, KPNO, and CFHT were considerably larger than those observed for the higher resolution observations. Part of this effect could be originated in the lower resolution of those spectra which affect the quality of the RV measurements due to the pair-blending effect, and additionally due to systematic RV differences between different data set. For this reason, CASLEO, KPNO, and CFHT data were excluded from the final orbital solution.

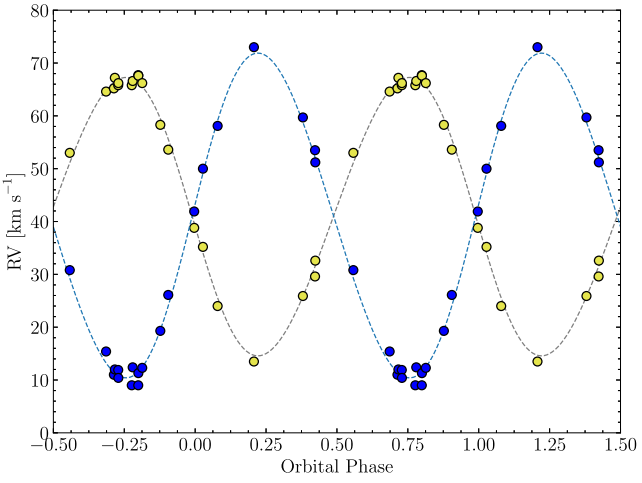

Figure 3. The spectroscopic orbital solution of HD 54662 AB derived using the GBART code. RVs of the primary component A (broad-lined) and secondary component B (narrow-lined) are represented by yellow and blue symbols, respectively. Orbital parameters are listed in Table 3. Error bars have similar size to symbols.

Table 3. Spectroscopic orbital elements for the binary HD 54662 AB obtained using the GBART code.

Parameter	Value
P (d)	2 102 ± 9
$V_{0\ \mathrm{AB}}$ (km s^{-1})	41.0 ± 0.2
K_{A} (km s^{-1})	26.4 ± 0.3
K_{B} (km s^{-1})	30.7 ± 0.3
e	0.055 ± 0.009
ω (°)	94.0 ± 9.3
T_{periast} (HJD)	2454 165 ± 55
T_{RVmax} (HJD)	2455 755 ± 55
$a_{\mathrm{A}} \sin i$ (km)	7.61 ± 0.13 × 10^8
$a_{\mathrm{B}} \sin i$ (km)	8.87 ± 0.14 × 10^8
$M_{\mathrm{A}} \sin^3 i$ ($\mathrm{M}_\odot$)	21.7 ± 1.3
$M_{\mathrm{B}} \sin^3 i$ ($\mathrm{M}_\odot$)	18.6 ± 1.3
q	0.857 ± 0.020
rms (km s^{-1})	1.25

The GBART code converges to a final orbital solution after a few iterations. The probable error of the orbital fit is 0.83 km s^{-1}. The fitted RV curves along with the RV measurements for both components are presented in Fig. 3, and the orbital elements derived from this fit are listed in Table 3.

4.2 The 3D orbit

We used the astrometric information provided by LB17 along with our RV measurements to compute a combined visual–spectroscopic orbit for HD 54662 AB. To this aim we used the IDL code ORBIT,[7] an

[5] https://exoplanetarchive.ipac.caltech.edu/docs/tools.html

[6] GBART is an improved version of the program for the determination of the orbital elements for spectroscopic binaries originally written by Bertiau & Grobben (1969), and updated in Bareilles (2017).

[7] The code is posted at https://doi.org/10.5281/zenodo.61119.

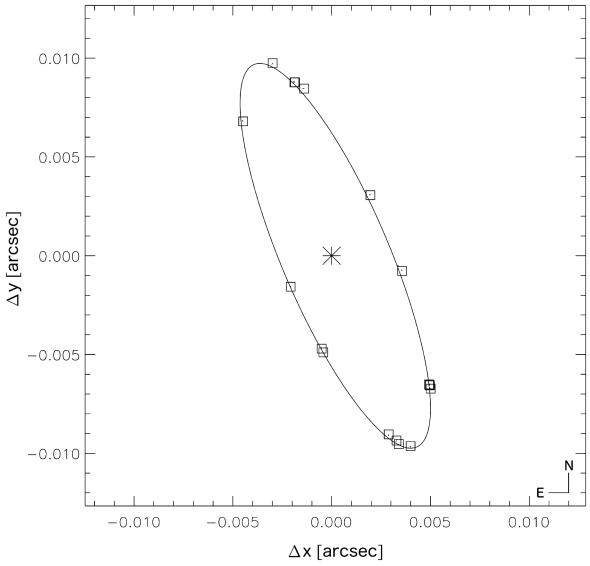

Figure 4. Apparent orbit of HD 54662 AB determined using the ORBIT code. The primary component A is at coordinates centre. Units are arcseconds. Parameters are listed in Table 4.

Table 4. Orbital elements for both components in HD 54662 AB obtained using ORBIT code.

Parameter	Value
P (d)	2113 ± 9
$V_{0\,AB}$ (km s^{-1})	41.5 ± 0.2
K_A (km s^{-1})	26.2 ± 0.3
K_B (km s^{-1})	30.7 ± 0.2
e	0.062 ± 0.008
i (°)	75.1 ± 0.5
Ω (°)	23.1 ± 0.4
ω (°)	83.3 ± 2.8
$T_{periast}$ (HJD)	2454 094 ± 18
T_{RVmax} (HJD)	2455 752 ± 18
a'' (mas)	10.5 ± 0.1
a_A (km)	7.86 ± 0.09 × 10^8
a_B (km)	9.21 ± 0.10 × 10^8
M_A ($M_\odot$)	23.8 ± 1.1
M_B ($M_\odot$)	20.3 ± 1.1
q	0.853 ± 0.018
rms_A (km s^{-1})	1.56
rms_B (km s^{-1})	1.34

interactive program developed by Andrei Tokovinin (see Tokovinin 1992). As a result we obtained a very robust solution, with relatively small errors. In Fig. 4, we show the apparent orbit obtained which can be compared with fig. A1 in LB17. The RV orbital solution obtained with ORBIT code is very similar to that determined with GBART code. The elements that characterize the combined orbit are listed in Table 4.

Our results are similar to the absolute orbital solutions previously determined (LB17, MMR18) in terms of eccentricity, orbital orientation and inclination, and total mass of the system, although there is a huge discrepancy in the values of the absolute masses of the components. This will be discussed in Section 6.3.

Table 5. Set of hydrogen and helium lines used in the quantitative spectroscopic analysis.

H I	He I	He II	He I + II
Hγ	4388	4200	4026
Hϵ	4471	4542	
	4713	4686	
	4922	5411	
	5876		

4.2.1 *Distance*

A dynamical distance to the binary can be estimated from the angular and linear sizes ($a'' = 10.5 \pm 0.1$ mas and $a_A + a_B = 17.07 \pm 0.1 \times 10^8$ km) of the orbit.

The resulting distance is 1087 ± 25 pc, in excellent agreement with the distance of $1170\pm^{120}_{100}$ pc obtained from the parallax measured by the *Gaia* mission, $\varpi = 0.8547 \pm 0.0799$ mas (published in the DR2; Brown et al. 2018), and the revised distance estimated by Bailer-Jones et al. (2018), $d = 1142\pm^{120}_{99}$ pc. Furthermore, we have determined a distance of $1157\pm^{121}_{39}$ using the method developed in Maíz Apellániz (2001, 2005), with parameters from Maíz Apellániz, Alfaro & Sota (2008), and including a parallax bias of -0.04 ± 0.01 mas.

We did an independent analysis of the dynamical distance using the new orbital fitting code presented by Maíz Apellániz (2019) and we found out that the *Gaia* distance is an overestimate of the dynamical distance by 5 per cent, which agrees with our result and is a difference of less than 1σ, lending more confidence to our results.

5 QUANTITATIVE SPECTROSCOPIC ANALYSIS

The spectral disentangling of the components of HD 54662 AB allowed us to compare each detached spectrum with model spectra in order to estimate the stellar and wind parameters. The quantitative analysis was performed by means of the IACOB Grid-Based Automatic Tool (IACOB-GBAT, see Simón-Díaz et al. 2011; Sabín-Sanjulián et al. 2014; Holgado et al. 2018). IACOB-GBAT uses a large grid of precomputed FASTWIND models (Santolaya-Rey, Puls & Herrero 1997; Puls et al. 2005) to compare automatically observed and synthetic H and He optical line profiles by means of a χ^2 algorithm. A solar metallicity ($Z = Z_\odot$) was adopted.

A list of the optical H and He lines used in the quantitative spectroscopic analysis of the components of HD 54662 AB is shown in Table 5. The same weight was given to each line. Note that not all the H Balmer diagnostic lines (the main diagnostic for surface gravity) were used in the analysis. The wings of H α and H β showed distortions in their shape due to residuals from the disentangling procedure (see Fig. 5). Moreover, the wings of H δ are blended with metallic lines (of N III and Si IV, mainly). Therefore, we only used Hγ and Hϵ lines for both stars.

5.1 Line broadening

The quantitative spectroscopic analysis with IACOB-GBAT requires the projected rotational velocity, $v \sin i$,[8] and the macroturbulence,

[8]Here, i is defined as the inclination angle of the rotation axis, which is not the same as the orbital inclination.

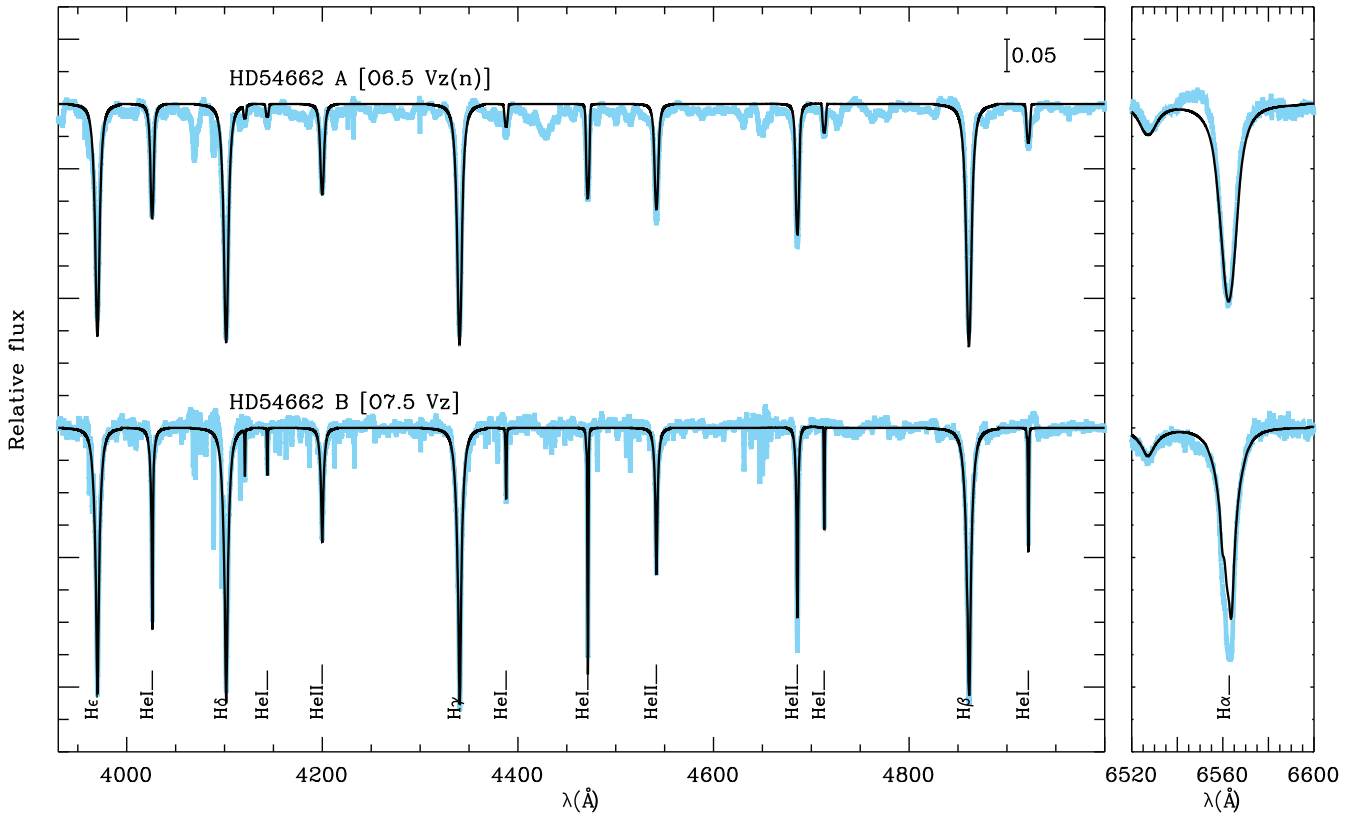

Figure 5. Individual spectra of the components of HD 54662 AB obtained from the disentangling procedure (in light blue). Each FASTWIND spectrum (in black) corresponds to the model from the IACOB-GBAT grid that best fits the observed spectrum. The usual optical H and He diagnostic lines are indicated (note that not all of them were used in the actual quantitative analysis, see Table 5).

$v_{\rm mac}$,[9] as input parameters. Thus, we used the IACOB-BROAD (Simón-Díaz & Herrero 2014), a tool that combines the Fourier Transform and the Goodness-of-Fit techniques, to characterize the broadening of the spectral lines of each component. We applied the tool to the O III λ5592 Å spectral line, which is present in both spectra. The results are shown in Table 6. For component A, we found a relatively high projected rotational velocity of 160 km s^{-1} in agreement with the spectral qualifier '(n)' (see Section 3.2). For component B, we measured a lower value for $v \sin i$ (∼40 km s^{-1}) and a similar value for macroturbulence. Simón-Díaz & Herrero (2014) showed that in the low $v \sin i$ regime (below ∼40 km s^{-1}), microturbulence could be playing a significant role in the broadening of the line, which tends to produce overestimates of $v \sin i$, while the derived value of $v_{\rm mac}$ is wholly attributable to microturbulence. Therefore, we considered the $v \sin i$ value of component B as an upper limit and fixed $v_{\rm mac}$ to zero.

5.2 Stellar and wind parameters

For each component of HD 54662 AB, the mean values and uncertainties of the following parameters were estimated: effective temperature $T_{\rm eff}$, surface gravity $\log g$, helium abundance $Y_{\rm He}$ (defined as N(He)/N(H)), microturbulence ξ_T, the β exponent of

[9]Simón-Díaz & Herrero (2014) showed that assuming a radial-tangential profile for macroturbulence in OB-type stars is appropriate for the estimation of $v \sin i$.

Table 6. Stellar parameters of both components in HD 54662 AB.

Parameter	Component A	Component B	Unit
Spectral types and absolute magnitudes (Sections 3.2 and 5.3)			
Sp. type	O6.5 V(n)z	O7.5 Vz	
M_V	−4.39 ± 0.12	−4.17 ± 0.12	mag
Line broadening parameters (Section 5.1)			
$v \sin i$	160 ± 18	≲40	km s^{-1}
$v_{\rm mac}$	40 ± 5	0	km s^{-1}
Atmospheric stellar parameters (Section 5.2)			
$T_{\rm eff}$	39.0 ± 0.5	39.0 ± 0.6	kK
$\log g$	3.97 ± 0.10	3.99 ± 0.10	dex
$\log g_{\rm c}$[a]	4.03 ± 0.10	4.00 ± 0.10	dex
$Y_{\rm He}$	0.10 ± 0.03	0.10 ± 0.03	
$\xi_{\rm T}$	14 ± 1	15 ± 3	km s^{-1}
$\log Q$	<−12.9	−12.7 ± 0.3	dex
Fundamental stellar parameters (Section 5.3)			
R	7.8 ± 0.1	7.1 ± 0.1	$R_\odot$
$\log L/L_\odot$	5.11 ± 0.11	5.02 ± 0.11	dex
$M_{\rm dy}$	23.8 ± 1.1	20.3 ± 1.1	$M_\odot$
$M_{\rm sp}$	23.9 ± 4.5	18.4 ± 4.2	$M_\odot$
$M_{\rm ev}$	29.6 ± 2.1	28.6 ± 1.8	$M_\odot$
Age	1.7 ± 0.7	1.6 ± 0.6	Ma

[a]Log $g_{\rm c}$ is the gravity corrected from rotational velocity defined as $\log g_{\rm c} = \log [g + (v \sin i)^2/R_*]$ (see e.g. Herrero et al. 1992; Repolust, Puls & Herrero 2004).

the wind velocity law, and the wind-strength Q-parameter.[10] The β exponent of the velocity law was fixed to 0.8, since the χ^2 distribution for this parameter was degenerate in both stars and it was not properly constrained. Table 6 presents the results.

Figs 5 and 6 illustrate the results of the quantitative spectroscopic analysis. In Fig. 5, the FASTWIND model that best fits the individual spectrum (in black) is compared with the disentangled spectrum of each component (in blue). In Fig. 6, the individual best-fitting models obtained from the analysis with IACOB-GBAT (in colour) and their addition (in black) are overlaid on one of the observed spectra of HD 54662 AB (in grey). The synthetic composite spectrum reproduces quite well the observed one for each H and He line. The values derived for stellar and wind parameters and their uncertainties are shown in Table 6.

5.3 Stellar radii, luminosities, and masses

The calculation of radii, and hence luminosities and spectroscopic masses ($M_{\rm sp}$), requires the knowledge of the absolute magnitude M_V of the analysed star. For each component, we calculated M_V from the apparent magnitude in the V band determined for the whole system ($m_V = 6.212$, Ducati et al. 2001) and the light contribution factors estimated in Section 3.1. We adopted the distance determined in Section 4 ($d = 1087 \pm 25$ pc) and a visual extinction of $A_V = 1.070 \pm 0.020$ (Maíz Apellániz & Barbá 2018). Additionally, present-day evolutionary masses ($M_{\rm ev}$) and ages were calculated using BONNSAI[11] (Schneider et al. 2014), a Bayesian tool that compares simultaneously all the available parameters (in our case, $v \sin i$, $T_{\rm eff}$, $\log g_{\rm c}$, and $\log L/L_\odot$, obtained with IACOB-GBAT) with evolutionary models from Brott et al. (2011) in the case of Galactic metallicity. Fundamental stellar parameters and their uncertainties are shown in Table 6 and discussed in the next section.

6 DISCUSSION

6.1 Orbital solution

There are similarities but also substantial differences between the new orbital solution determined in Section 4 and the orbits previously obtained for HD 54662 AB.

Our orbital period and eccentricity ($P = 2113 \pm 9$ d and $e = 0.062 \pm 0.009$) are of course different to the historical ones found by B07, a fact that can be attributed to the better temporal and phase coverage of the new data. Our determinations are very similar to the values more recently calculated by LB17 and MMR18.

The most important difference arises in the orbital semi-amplitudes and, consequently, in the minimum masses computed for both stars, which will be discussed below. B07 estimated the projected rotational velocity, $v \sin i$, of the broad-lined component (which they identified as the secondary) to be 110 km s^{-1}, which is significantly smaller than our value (160 km s^{-1}; Table 6). This leads to RV measurements which subsequently overestimate the RV semi-amplitudes. The discrepancy with the orbit calculated by LB17 has a similar origin. Furthermore, we should to remark that these authors derived a total mass of the system from the astrometric orbit and distance of about $45 \pm 12\,M_\odot$, which is in good concordance with the total mass determined in our orbital solution of $44.1 \pm 2.2\,M_\odot$. The differences in the masses determination between our results and MMR18 is discussed below.

6.2 Stellar parameters

Our individual classifications are in good agreement with the spectral classification derived for the system as a whole (O7 Vz var; Sota et al. 2014). However, we conclude that the broad-lined star has the earlier spectral type, thus being the most massive of the two components, in contrast to the results presented by B07 and MMR18.

In Section 5, modern stellar atmosphere models were compared to the disentangled spectra of each component of HD 54662 AB in order to estimate their physical parameters. A previous quantitative spectroscopic study of the system components was performed by MMR18 using the CMFGEN code (Hillier & Miller 1998).

Regarding the projected rotational velocities, using the Fourier Transform method (Simón-Díaz & Herrero 2007) MMR18 determined 158 and 43 km s^{-1} for the *genuine*[12] primary (A) and secondary (B) components, respectively. These values perfectly agree with our determinations of $v \sin i$ (see Table 6). However, we differ with the former authors regarding the macroturbulent velocity: while MMR18 attributed to component B a macroturbulence of 35 km s^{-1} in order to match the observed line profiles with the synthetic spectra, we estimated a macroturbulence of 40 km s^{-1} for component A and fixed this parameter to zero for component B, since we found no reason to modify its value when checking the broadening of the synthetic line profiles.

The values computed in this work for the effective temperatures ($T_{\rm eff}$) and surface gravities ($\log g$) of the components are consistent, within the uncertainties, with the current calibrations for O stars in the Milky Way, including the classical calibration by Martins et al. (2005), as well as the most recent ones by Simón-Díaz et al. (2014) and Holgado et al. (2018). MMR18 also determined $T_{\rm eff}$, as well as helium abundances ($Y_{\rm He}$) for both stars. While our estimates of $\log g$ and $Y_{\rm He}$ are in good agreement with their values, our $T_{\rm eff}$ determinations result in slightly higher values than theirs ($\Delta T_{\rm eff} \approx 1500$ K). We re-analysed both stars using the line broadening parameters estimated by MMR18. We obtained good agreement for component A, in contrast to component B. Moreover, the broadening of the FASTWIND synthetic lines using MMR18's $v \sin i$ and $v_{\rm mac}$ values cannot reconcile the broadening of the lines observed in our disentangled spectra. Therefore, line broadening only cannot explain the differences in $T_{\rm eff}$ with MMR18.

In Section 3.1, we mentioned that the presence of residuals in the Balmer lines originated from the disentangling process may affect the surface gravity determination. As explained in Section 5, for our analysis we used the least affected lines (Hγ and Hϵ) in order to minimize this effect. Regarding the He lines, some profile distortions which could be playing a role are also observed, in particular in the He I λ 4388 Å line, mostly for the primary component. In any case, Fig. 6 shows that the synthetic composite spectrum resulting from the addition of the individual models for the A and B components reproduces well the observed spectrum of the system. We then conclude that potential differences in the shape of the lines of the individual spectra due to different disentangling processes may be

[10] $Q = \dot{M}(R v_\infty)^{-1.5}$, where $\dot{M}$ is the mass-loss rate, R is the stellar radius, and v_∞ is the terminal velocity of the wind (see Puls et al. 1996).

[11] The BONNSAI web-service is available at www.astro.uni-bonn.de/stars/bonnsai.

[12] We recall that MMR18 adopted the identification from B07 in which the broad-lined star was the secondary component, here demonstrated to be wrong.

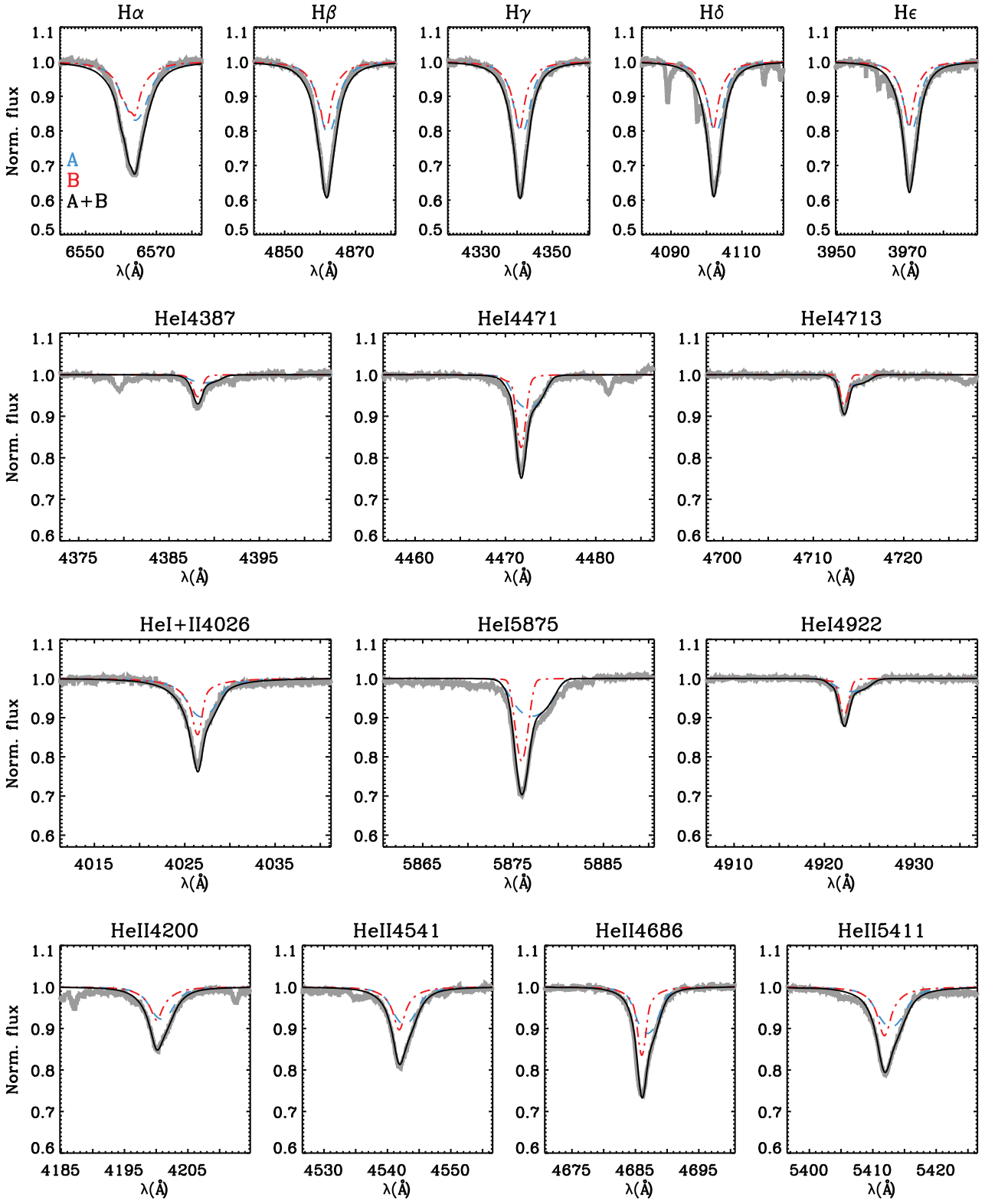

Figure 6. Observed FEROS spectrum of HD 54662 AB (in grey) compared to individual and combined synthetic models from the analysis with IACOB-GBAT. Blue dashed and red dot–dashed lines correspond to the best-fitting FASTWIND models ($T_{\rm eff}$ = 39 kK, $\log g$ = 3.90 dex, and $\log Q$ = –13.0 for component A; $T_{\rm eff}$ = 39 kK, $\log g$ = 4.00 dex, and $\log Q$ = –13.0 for component B), diluted according to brightness factors (0.55 and 0.45 for components A and B, respectively). Individual models were added in order to obtain a combined FASTWIND spectrum (black line) to compare with the observed one. All FASTWIND models in this figure have $Y_{\rm He}$ = 0.09 and β = 0.8.

the cause of the disagreement between our determinations and those from MMR18. Note also that, unlike the results presented here, the former authors classified both components as O6.5 and estimated a difference in M_V of 0.75 mag between them, which suggests a difference in the intensity of the He lines with respect to our spectra.

6.3 Stellar masses

In spectroscopic binaries the mass determinations strongly depend on the measured radial velocity semi-amplitudes. Using the RVs from B07, LB17 obtained unrealistic masses of 58 ± 16 and 316 ± 168 $M_\odot$ for the A and B components, respectively, claiming themselves to consider these values with caution. On the opposite extreme are the masses derived from the orbital solution by MMR18. In the former study, as in the present one, a spectral disentangling was used to determine the RVs and individual spectra of each star, although MMR18 obtained minimum masses of 7.3 and 8.7 $M_\odot$ for the A and B stars, respectively, significantly lower than the values derived in this work. When combined with the orbital inclination determined in LB17, MMR18 obtained absolute masses of 9.7 and 8.2 $M_\odot$, 'surprisingly low for O-type stars'. In this work, we inferred $M_A = 23.8\,M_\odot$ and $M_B = 20.3\,M_\odot$. Thus, our dynamical masses are in agreement with those expected from the spectral types.

We estimated the stellar masses of the two components of HD 54662 AB using three different methods. First, we calculated absolute dynamical masses (M_{dyn}) combining our radial velocity measurements and the available astrometric data (Section 4). Secondly, we inferred spectroscopic masses (M_{sp}) through the comparison of the disentangled spectra with FASTWIND atmosphere models. Finally, we determined evolutionary masses (M_{ev}) comparing the physical parameters derived for the stellar components with theoretical models of stellar evolution (Section 5.3). Table 6 summarizes these results.

As shown in Table 6, in the three cases the star A is more massive than the star B, as expected according to the spectral classification and the mass ratio derived from the orbital solution ($q = 0.85 \pm 0.02$, Section 4). Spectroscopic and dynamical masses agree among themselves within the error bars. When compared to the calibrations of stellar parameters for Galactic O stars (e.g. Martins et al. 2005), these values are somewhat smaller than *expected* for an O6.5 and an O7.5 dwarfs. However, a significant difference with respect to the evolutionary mass is observed. For both components, the evolutionary masses are around 1.2–1.5 times larger than the dynamical and spectroscopic masses ($M_{ev} \sim 1.2$–$1.5\,M_{dyn,sp}$). This may be related to a long-standing problem in the field of massive stars known as the *mass discrepancy problem*, i.e. where the calculated evolutionary masses are systematically larger than the spectroscopically derived masses (Herrero et al. 1992; Herrero, Puls & Najarro 2002). Recently, Sabín-Sanjulián et al. (2017) in the LMC and Markova, Puls & Langer (2018) in the MW showed that mass discrepancy is present in environments of different metallicity. They also show that in the 'low-mass' regime (M_* within the approximate range 20–30 $M_\odot$), the effect is such that spectroscopic masses tend to be smaller than evolutionary ones. Markova et al. (2018) pointed to a wrong treatment of microturbulence in the stellar atmosphere models as a possible source of the discrepancy. Nevertheless in the case of HD 54662 AB, the spectroscopic masses are in good agreement with the model-independent dynamical masses, which can be accurately determined using elemental physical laws. A detailed quantitative study of a statistically significant number of massive binaries will be necessary to clarify this question.

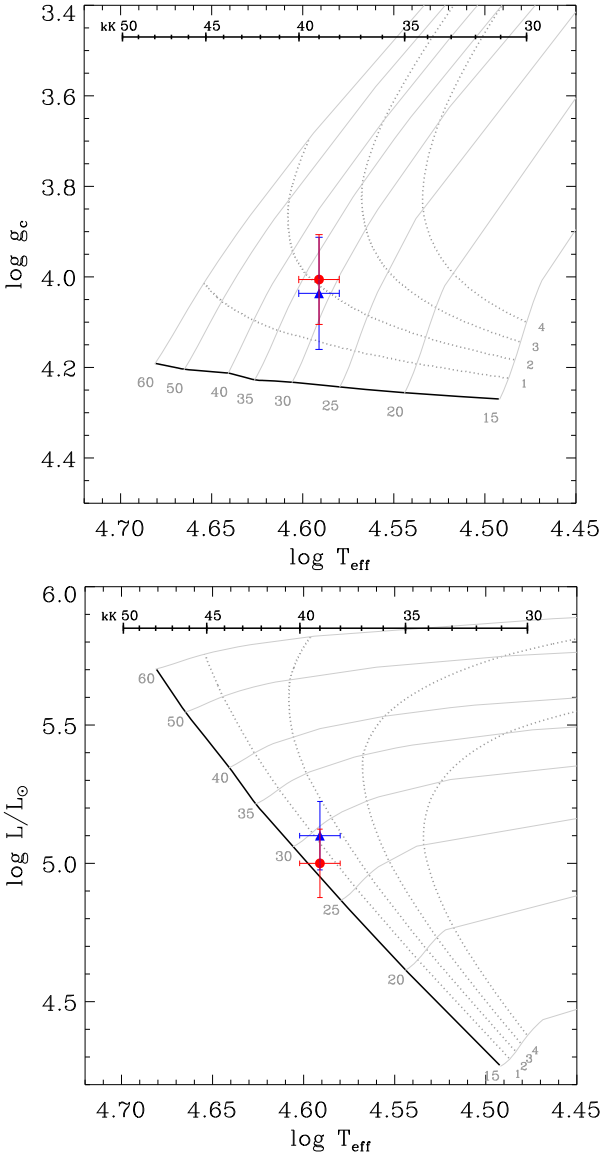

Figure 7. Location of both components of HD 54662 AB in the Kiel (top) and HR (bottom) diagrams (blue triangle and red circle correspond to components A and B, respectively). Evolutionary tracks and isochrones for isolated stars with Galactic metallicity are taken from Brott et al. (2011), for which an initial rotational velocity $v_{ini} = 166$ km s^{-1} was selected. Initial stellar masses (in solar masses) and ages (in Ma) are shown for evolutionary tracks and isochrones, respectively. The ZAMS is indicated by the bold black line. Estimated error bars for each star are also shown.

6.4 Evolutionary status

Fig. 7 presents the position of the two components of HD 54662 AB in the Kiel diagram and in the Hertzsprung–Russell (HR) diagram, according to the stellar parameters derived in Section 5. Evolutionary tracks computed for main-sequence *single* stars, i.e. stars that evolve without any kind of binary interaction, were considered. This is valid because, in contrast to close binaries, the large orbital period and wide separation of the system reduce significantly the possibilities of an interaction between both stars (see e.g. de Mink, Pols & Hilditch 2007; Langer 2012). HD 54662 AB is thus a binary system suitable to be used as a test-bed for evolutionary models of single stars (Brott et al. 2011).

As seen in Fig. 7, the location with respect to evolutionary tracks and isochrones of both stars in the Kiel and HR diagrams are somewhat different. In the former, both stars appear more massive than in the latter, a discrepancy already noted by Sabín-Sanjulián et al. (2017) and Markova et al. (2018), and for which a compelling explanation has not been found yet. In any case, the use of the BONNSAI tool, which takes into account all the available parameters (Section 5.3), allowed us to obtain reliable masses and ages.

In both, the Kiel and the HR diagrams, the two stars are located relatively close to the zero-age main sequence (ZAMS), with ages below ∼2.5 Ma. The youth of the components and the presence of relatively thin winds (especially in component A, see Section 5.2) agree well with their Vz nature (see Sabín-Sanjulián et al. 2014; Arias et al. 2016, and references therein).

An important point to remark is the difference in the projected rotational velocities of both components. This behaviour could be related to asynchronously rotating components, so it becomes crucial to consider both phenomena when computing evolutionary models of binary systems.

7 SUMMARY AND OUTLOOK

In this paper, we presented a detailed study of the long-period massive binary HD 54662 AB. A spectral disentangling technique was applied to recover the individual spectra of the primary (A) and the secondary component (B), which were classified as O6.5 V(n)z and O7.5 Vz, respectively. Contrary to previous studies, the primary, i.e. the most massive object of the system, was demonstrated to be the star with the broadest spectral lines.

A new 3D orbital solution for HD 54662 AB was determined by combining RV measurements and astrometric data from LB17. The orbit thus obtained is characterized by a period $P = 2113 \pm 9$ d (5.79 yr), a very small eccentricity ($e = 0.06$), and an inclination $i = 75.1^{\circ}$. Together with 9 Sgr AB ($P = 2900$ d; Rauw et al. 2012) and HD 191612 AB ($P = 1542$ d; Howarth et al. 2007), HD 54662 AB is one of the three rare spectroscopic O + O/B systems with periods longer than 1000 d known to date. Contrary to HD 54662 AB, the orbit of 9 Sgr AB exhibits a high eccentricity, but also presents a composite spectrum showing a narrow and a broad component (Rauw et al. 2005, 2012). Absolute dynamical masses of $M_{\rm A} = 23.8 \pm 1.1$ M$_{\odot}$ and $M_{\rm B} = 20.3 \pm 1.1$ M$_{\odot}$ were obtained by means of the ORBIT code.

Quantitative spectroscopic analysis was performed on the disentangled spectra in order to determine the physical properties of the individual components. FASTWIND stellar atmosphere models and the IACOB-GBAT tool were used to this aim. Evolutionary masses and ages were also computed by means of the Bayesian tool BONNSAI. Most of the stellar parameters determined in this work are consistent with the current calibrations for Galactic O dwarfs.

While the values derived for the dynamical (model-independent) and spectroscopic masses agree well between themselves, the evolutionary masses are 20 – 50 per cent higher. This may be related to the *mass discrepancy problem*. A detailed study which provides accurate values for dynamical, spectroscopic, and evolutionary masses of a large number of O-type stars is crucial to shed some light on this issue. Both components have ages below 2.5 Ma. Their young age and the presence of thin winds are consistent with the Vz nature of the two stars.

We emphasize that, in spite of the above discussed, dynamical and spectroscopic mass determinations derived in this work are in reasonable agreement with what it is expected for the components of HD 54662 AB.

A remarkable characteristic of HD 54662 AB is the large difference (by a factor of 4) between the projected rotational velocities measured for the primary and secondary, namely, 160 and $\lesssim$40 km s^{-1}, respectively. The *OWN Survey* has discovered several massive systems with such characteristic, which are currently under analysis (see e.g. Putkuri et al. 2018). Taking into account the youthful age of the system, this difference is very likely connected to the amount and direction of the angular momentum at the time of birth, since the components have probably not experiencing tidal synchronization or mass transfer yet. The stars could have formed with very different rotational velocities and/or non-parallel rotation axes. Thus, this system offers the opportunity to test the different scenarios of formation and evolution of massive multiple systems.

ACKNOWLEDGEMENTS

We thank the anonymous reviewer, who did a thorough reading, which helped to improve the manuscript. Also, we thank the directors and staff at CASLEO, LCO, La Silla, and KPNO for the use of their facilities and their kind hospitality during the observing runs. RG, GF and CP are visiting Astronomers of Complejo Astronómico El Leoncito. CS-S acknowledges support from CONICYT-Chile through the FONDECYT Postdoctoral Project 3170778. The Space Telescope Science Institute is operated by the Association of Universities for Research in Astronomy Inc., under NASA contract NAS5-26555. TSB acknowledges support provided through NASA grant ADAP12-0172. MVM is supported by the National Science Foundation under grant AST-1109247 and an institutional grant from Lehigh University. This research has made use of the NASA's Astrophysics Data System and the SIMBAD data base (operated at CDS, Strasbourg, France), and ESO's Science Archive. JIA and RHB acknowledge financial support from the Dirección de Investigación y Desarrollo de la Universidad de La Serena through project PR16142 and PR18143, respectively.

This study is based on observations collected at: Las Campanas Observatory (LCO) including the 6–5 m Magellan telescopes; the European Organisation for Astronomical Research in the Southern Hemisphere (programmes: 081.D-2008, 086.D-0997, 087.D-0946); the Complejo Astronómico El Leoncito (CASLEO), operated under agreement between the Consejo Nacional de Investigaciones Científicas y Técnicas de la República Argentina and the National Universities of La Plata, Córdoba, and San Juan; and the Kitt Peak National Observatory (KPNO).

REFERENCES

Arias J. I. et al., 2016, AJ, 152, 31
Bailer-Jones C. A. L., Rybizki J., Fouesneau M., Mantelet G., Andrae R., 2018, AJ, 156, 58
Barbá R. H., Gamen R., Arias J. I., Morrell N. I., 2017, in Eldridge J. J., Bray J. C., McClelland L. A. S., Xiao L., eds, IAU Symp. Vol. 329, The Lives and Death-Throes of Massive Stars, Cambridge University Press, Cambridge, p. 89
Barbá R. H., Gamen R., Arias J. I., Morrell N. I., Maíz Apellániz J., Alfaro E., Walborn N., Sota A., 2010, Rev. Mex. Astron. Astrofis. Conf. Ser., 38, 30
Bareilles F., 2017, Astrophysics Source Code Library, record ascl:1710.014
Bernstein R., Shectman S. A., Gunnels S. M., Mochnacki S., Athey A. E., 2003, in Iye M., Moorwood A. F. M., eds, Proc. SPIE Conf. Ser. Vol. 4841, Instrument Design and Performance for Optical/Infrared Ground-Based Telescopes. SPIE, Bellingham, p. 1694
Bertiau F. C., Grobben J., 1969, Ric. Astron., 8, 1
Boyajian T. S. et al., 2007, ApJ, 664, 1121

Brott I. et al., 2011, A&A, 530, A115
Brown A. G. A. et al., 2018, A&A, 616, A1
Conti P. S., Leep E. M., Lorre J. J., 1977, ApJ, 214, 759
Dekker H., D'Odorico S., Kaufer A., Delabre B., Kotzlowski H., 2000, in Iye M., Moorwood A. F., eds, Proc. SPIE Conf. Ser. Vol. 4008, Optical and IR Telescope Instrumentation and Detectors. SPIE, Bellingham, p. 534
de Mink S. E., Pols O. R., Hilditch R. W., 2007, A&A, 467, 1181
Ducati J. R., Bevilacqua C. M., Rembold S. B., Ribeiro D., 2001, ApJ, 558, 309
Fullerton A. W., 1990, PhD thesis, Toronto Univ., Ontario
Garmany C. D., Conti P. S., Massey P., 1980, ApJ, 242, 1063
González J. F., Levato H., 2006, A&A, 448, 283
Herrero A., Kudritzki R. P., Vilchez J. M., Kunze D., Butler K., Haser S., 1992, A&A, 261, 209
Herrero A., Puls J., Najarro F., 2002, A&A, 396, 949
Hillier D. J., Miller D. L., 1998, ApJ, 496, 407
Holgado G. et al., 2018, A&A, 613, A65
Howarth I. D. et al., 2007, MNRAS, 381, 433
Kaufer A., Stahl O., Tubbesing S., Nørregaard P., Avila G., Francois P., Pasquini L., Pizzella A., 1999, The Messenger, 95, 8
Langer N., 2012, ARA&A, 50, 107
Lanz T., Hubeny I., 2003, ApJS, 146, 417
Le Bouquin J.-B. et al., 2017, A&A, 601, A34
Markova N., Puls J., Langer N., 2018, A&A, 613, A12
Marraco H. G., Muzzio J. C., 1980, PASP, 92, 700
Martins F., Plez B., 2006, A&A, 457, 637
Martins F., Schaerer D., Hillier D. J., Meynadier F., Heydari-Malayeri M., Walborn N. R., 2005, A&A, 441, 735
Maíz Apellániz J., 2001, AJ, 121, 2737
Maíz Apellániz J., 2005, in Turon C., O'Flaherty K. S., Perryman M. A. C., eds, ESA SP-576: The Three-Dimensional Universe with Gaia. ESA, Noordwijk, p. 179
Maíz Apellániz J., 2019, A&A, 630, A119
Maíz Apellániz J., Alfaro E. J., Sota A., 2008, preprint (arXiv:0804.2553)
Maíz Apellániz J., Barbá R. H., 2018, A&A, 613, A9
Maíz Apellániz J., et al., 2016, ApJS, 224, 4
Maíz Apellániz J. et al., 2012, in Drissen L., Rubert C., St-Louis N., Moffat A. F. J., eds, ASP Conf. Ser. Vol. 465, Proceedings of a Scientific Meeting in Honor of Anthony F. J. Moffat. Astron. Soc. Pac., San Francisco, p. 484
Mossoux E., Mahy L., Rauw G., 2018, A&A, 615, A19
Plaskett J. S., 1924, Publ. Dom. Astrophys. Obs. Victoria, 2, 287
Puls J., Urbaneja M. A., Venero R., Repolust T., Springmann U., Jokuthy A., Mokiem M. R., 2005, A&A, 435, 669
Puls J. et al., 1996, A&A, 305, 171
Putkuri C., Gamen R., Morrell N. I., Simón-Díaz S., Barbá R. H., Ferrero G. A., Arias J. I., Solivella G., 2018, A&A, 618, A174
Rauw G., Sana H., Gosset E., De Becker M., Arias J., Morrell N., Eenens P., Stickland D., 2005, in Rauw G., Nazé Y., Blomme R., Gosset E., eds, Massive Stars and High-Energy Emission in OB Associations, a workshop of the JENAM 2005, "Distant Worlds", held in Liège (Belgium), p. 85
Rauw G., Sana H., Spano M., Gosset E., Mahy I., De Becker M., Eenens P., 2012, A&A, 542, A95
Repolust T., Puls J., Herrero A., 2004, A&A, 415, 349
Sabín-Sanjulián C. et al., 2014, A&A, 564, A39
Sabín-Sanjulián C. et al., 2017, A&A, 601, A79
Sana H. et al., 2012, Science, 337, 444
Sana H. et al., 2014, ApJS, 215, 15
Santolaya-Rey A. E., Puls J., Herrero A., 1997, A&A, 323, 488
Scargle J. D., 1982, ApJ, 263, 835
Schneider F. R. N., Langer N., de Koter A., Brott I., Izzard R. G., Lau H. H. B., 2014, A&A, 570, A66
Simón-Díaz S., Castro N., Herrero A., Puls J., Garcia M., Sabín-Sanjulián C., 2011, J. Phys. Conf. Ser., 328, 012021
Simón-Díaz S., Herrero A., 2007, A&A, 468, 1063
Simón-Díaz S., Herrero A., 2014, A&A, 562, A135
Simón-Díaz S., Herrero A., Sabín-Sanjulián C., Najarro F., Garcia M., Puls J., Castro N., Evans C. J., 2014, A&A, 570, L6
Sota A., Maíz Apellániz J., Morrell N. I., Barbá R. H., Walborn N. R., Gamen R. C., Arias J. I., Alfaro E. J., 2014, ApJS, 211, 10
Sota A., Maíz Apellániz J., Walborn N. R., Alfaro E. J., Barbá R. H., Morrell N. I., Gamen R. C., Arias J. I., 2011, ApJS, 193, 24
Stickland D. J., Lloyd C., 2001, The Observatory, 121, 1
Tokovinin A., 1992, in McAlister H. A., Hartkopf W. I., eds, ASP Conf. Ser. Vol. 32, IAU Colloq. 135: Complementary Approaches to Double and Multiple Star Research. Astron. Soc. Pac., San Francisco, p. 573

APPENDIX A

Table A1. Radial velocities for both components in HD 54662 AB determined from CASLEO spectra.

HJD 2,400,000+	RV_A (km s^{-1})	σ_A (km s^{-1})	RV_B (km s^{-1})	σ_B (km s^{-1})
53 866.489	60.7	4.2	25.5	2.8
54 220.467	43.0	4.4	52.7	3.3
54 478.623	24.5	3.7	76.1	3.3
54 508.593	1.6	5.3	77.1	4.1
54 842.646	8.9	4.0	69.3	2.6
54 847.590	19.0	4.4	71.2	2.9
54 963.509	25.9	1.6	59.7	1.0
54 984.446	16.6	4.1	63.9	3.3
55 896.680	50.4	4.4	18.0	3.2
55 897.650	55.6	4.0	18.9	3.2
55 925.606	58.5	4.4	23.5	3.3
57 078.544	17.3	4.6	62.3	3.3
57 087.530	17.1	4.0	61.0	3.4

Table A2. Radial velocities for both components in HD 54662 AB, determined from CFHT and KPNO spectra. Rows 1–17: CFHT data used in (Fullerton 1990). Rows 18–51: KPNO data used in B07. Rows 52–55: new KPNO data.

HJD 2400 000+	RV_A (km s^{-1})	RV_B (km s^{-1})
46 426.830	22.5	61.5
46 426.904	23.4	61.2
46 426.980	24.2	61.7
46 427.802	24.4	61.2
46 427.869	25.3	61.3
46 427.925	24.0	61.3
46 427.973	25.5	61.3
46 428.036	25.8	61.7
46 428.132	24.4	61.2
46 428.805	25.0	62.4
46 429.021	25.7	61.8
46 429.814	24.3	61.6
46 429.883	25.1	61.1
46 432.853	25.3	61.6
46 432.897	25.2	61.1
46 432.999	25.5	61.4
46 433.093	24.6	61.6
51 817.967	70.4	21.4
51 818.962	64.5	19.9
51 819.962	63.0	21.4
51 820.990	65.6	19.5
51 821.968	67.5	16.4
51 822.941	64.3	22.2
51 823.957	71.1	19.6
51 824.903	65.6	21.4
51 889.990	70.4	23.3
51 890.923	64.5	23.4
51 892.899	61.5	22.8
51 893.926	60.4	26.8
51 894.882	65.5	23.7
51 894.956	66.0	27.2
51 895.934	59.6	27.7
51 896.033	62.2	26.6
51 896.881	60.6	25.7
51 896.952	58.2	25.3
51 897.879	63.7	25.2
51 897.943	63.2	23.3
51 898.891	71.5	27.6
51 898.953	66.6	27.7
51 899.885	61.5	25.7
51 899.947	61.3	24.9
51 900.878	67.3	27.0
51 900.940	64.5	25.7
51 901.885	68.6	22.0
51 901.949	63.8	28.6
54 020.025	68.3	33.9
54 024.964	68.9	30.7
54 027.025	50.5	34.4
54 028.964	50.6	34.6
54 030.961	54.4	35.3
54 032.012	52.8	36.5
54 758.993	17.5	67.6
54 779.030	25.7	65.4
54 783.037	22.0	65.3
55 911.960	68.8	14.8

This paper has been typeset from a TEX/LATEX file prepared by the author.